CANCER

CytoPAN—Portable cellular analyses for rapid point-of-care cancer diagnosis

Jouha Min[1]*, Lip Ket Chin[1,2]*, Juhyun Oh[1], Christian Landeros[1,3], Claudio Vinegoni[1], Jeeyeon Lee[4], Soo Jung Lee[5], Jee Young Park[6], Ai-Qun Liu[2], Cesar M. Castro[1,7], Hakho Lee[1,8†], Hyungsoon Im[1,8†], Ralph Weissleder[1,8,9†]

Rapid, automated, point-of-care cellular diagnosis of cancer remains difficult in remote settings due to lack of specialists and medical infrastructure. To address the need for same-day diagnosis, we developed an automated image cytometry system (CytoPAN) that allows rapid breast cancer diagnosis of scant cellular specimens obtained by fine needle aspiration (FNA) of palpable mass lesions. The system is devoid of moving parts for stable operations, harnesses optimized antibody kits for multiplexed analysis, and offers a user-friendly interface with automated analysis for rapid diagnoses. Through extensive optimization and validation using cell lines and mouse models, we established breast cancer diagnosis and receptor subtyping in 1 hour using as few as 50 harvested cells. In a prospective patient cohort study ($n = 68$), we showed that the diagnostic accuracy was 100% for cancer detection and the receptor subtyping accuracy was 96% for human epidermal growth factor receptor 2 and 93% for hormonal receptors (ER/PR), two key biomarkers associated with breast cancer. A combination of FNA and CytoPAN offers faster, less invasive cancer diagnoses than the current standard (core biopsy and histopathology). This approach should enable the ability to more rapidly diagnose breast cancer in global and remote settings.

INTRODUCTION

The global cancer burden has risen to 18.1 million new cases in 2018 and is projected to reach 29.5 million new cases by 2040 (*1*, *2*). In 2018, there were 9.6 million cancer deaths, making cancer the cause of death for 1 in 8 men and 1 in 11 women. More than two-thirds of cancer deaths occur in low- and middle-income countries (LMICs). These numbers have been steadily increasing due to population growth, aging, and viral infections (such as HIV, human papillomavirus, and hepatitis). However, these increases are also due to shifting social and economic development (*3*, *4*). For example, in rapidly growing economies, there is a shift from cancers related to poverty and infections to cancers associated with lifestyles typically found in industrialized countries. Furthermore, in sub-Saharan African countries with successful HIV therapies, cancer incidence is rising (*5*–*7*).

Efficient screening and early cancer detection programs using mammography are commonplace in developed countries. Furthermore, biomarker analyses in serum (liquid biopsies) are emerging, and genomic biomarker analyses are beginning to be implemented for cancer diagnostics. In LMICs, however, a cancer diagnosis often occurs after advanced symptoms, for example, palpable mass lesions, weight loss, and malaise. It is not uncommon for biopsy diagnoses to take several months, given the lack of surgeons, interventionalists, and pathologists, bottlenecks in specimen acquisition, complex handling logistics, and other factors (*8*). For example, in 2017, only a quarter of low-income countries reported having generally available public sector pathology services (*9*). All of this may lead to delayed diagnoses, missed treatment options, and increased mortality rates.

For women with suspicion of breast cancer, preoperative assessment of focal lesions in the breasts is crucial in the planning of further therapeutic management. Pathology information includes the presence of estrogen receptors (ERs) and progesterone receptors (PRs), human epidermal growth factor receptor 2 (HER2) status, presence of invasion, histological type, and tumor grade. For example, treatment of women with nonmetastatic, ER-positive disease with tamoxifen, or aromatase inhibitors decreases cancer recurrence and mortality (*10*). In LMICs, tamoxifen is commonly included on national essential medicine lists (*11*). The generic drug is readily available at a low cost, and, in some countries, it is available free of charge (*12*). Nevertheless, the benefits of this drug cannot be realized without knowledge of hormone receptor status.

To address the above problems of delayed diagnoses, we and others have been interested in devising automated, rapid, portable, and affordable diagnostic and profiling technologies. Some previous developments have harnessed innovations in micro–nuclear magnetic resonance (μNMR) (*13*), electrochemical sensing (*14*), nanoplasmonic sensing (*15*, *16*), and holography (*17*, *18*). Other research teams have developed biosensors and analytical technologies for point-of-care (POC) applications, leveraging electrical, optical, calorimetric, and electrochemical transducer systems (*19*–*26*).

Although these earlier systems can perform diagnoses in an optimized laboratory setting, field testing in LMICs has revealed several additional prerequisites for successful cancer diagnosis. These include the growing realization that technologies should (i) produce actionable results within a day (and ideally within 1 to 2 hours) to minimize loss of patient follow-up, (ii) use cellular rather than tissue specimens

[1]Center for Systems Biology, Massachusetts General Hospital, Boston, MA 02114, USA. [2]School of Electrical and Electronic Engineering, Nanyang Technological University, Singapore 639798, Singapore. [3]Harvard-MIT Program in Health Sciences and Technology, Massachusetts Institute of Technology, Cambridge, MA 02139, USA. [4]Department of Surgery, School of Medicine, Kyungpook National University, Kyungpook National University Chilgok Hospital, Daegu 41404, Republic of Korea. [5]Department of Oncology/Hematology, School of Medicine, Kyungpook National University, Kyungpook National University Chilgok Hospital, Daegu 41404, Republic of Korea. [6]Department of Pathology, School of Medicine, Kyungpook National University, Kyungpook National University Chilgok Hospital, Daegu 41404, Republic of Korea. [7]Cancer Center, Massachusetts General Hospital, Boston, MA 02114, USA. [8]Department of Radiology, Massachusetts General Hospital, Boston, MA 02114, USA. [9]Department of Systems Biology, Harvard Medical School, Boston, MA 02115, USA.
*These authors contributed equally to the manuscript.
†Corresponding author. Email: rweissleder@mgh.harvard.edu (R.W.); im.hyungsoon@mgh.harvard.edu (H.I.); hlee@mgh.harvard.edu (H.L.)

to avoid lengthy embedding and staining procedures, (iii) profile a large number of cells for multiple markers, (iv) automate readouts to avoid bottlenecks in specialist interpretation, (v) incorporate self-calibration and quality controls, and (vi) be accompanied by prepackaged lyophilized kits containing all necessary reagents for onsite sample processing outside of specialty labs.

Here, we report the development and validation of an affordable image cytometry system that allows automated and same-day molecular analyses of fine needle aspiration (FNA) specimens. Termed CytoPAN, for portable fluorescence-based image cytometry analyzer, the system performs multichannel imaging for cancer diagnosis and subtyping. A set of images is then analyzed via custom-developed algorithms for fast, accurate, and automated cellular profiling without user input. We designed the system to allow multiplexed detection in five different channels, prepared lyophilized kits containing relevant antibodies, and optimized assays for the molecular analysis of breast cancer in cell lines and mouse models. After these discovery efforts and mouse co-clinical trials, we applied the system to a human validation cohort. This cohort included 68 patients who underwent preoperative FNA of breast lesions and subsequent surgery with pathological workup as the gold standard.

RESULTS

Overall design criteria and analysis procedure

The CytoPAN system is designed to comply with the "ASSURED" (affordable, sensitive, specific, user-friendly, rapid and robust, equipment-free, and deliverable to end users) criteria outlined by the World Health Organization for evaluating POC devices for resource-limited environments (*27*, *28*). Figure 1 highlights the overall workflow of CytoPAN analyses. First, cells are collected through minimally invasive FNAs and immunostained against multiple biomarkers of interest using lyophilized immunostaining kits containing the relevant antibodies. The lyophilized kits are essential to deploy the approach in resource limited settings without access to refrigeration. In a typical clinical setting, each single needle pass (20 to 22 gauge) provides about 10^2 to 10^5 cells, depending on technique and type of lesion (*29*). The stained cells are mounted in a designated area of a glass substrate and imaged by the CytoPAN device. A custom-developed automatic analysis algorithm is then applied for cell segmentation, expression level thresholding, and cellular analysis, and the end results are displayed on the user interface. The FNA-CytoPAN diagnostic procedure is completed within an hour, substantially faster than the core biopsy and histopathology (fig. S1) and considerably shorter than the median turnaround time of 160 days in some resource-constrained regions (*30*).

To identify breast cancer cells, we used a quad-marker signature (Quad) to identify cancer cells, as well as CD45 and size to identify host cells. The Quad signature includes epithelial cell adhesion molecule (EpCAM), epidermal growth factor receptor (EGFR), mucin-1 (MUC1), and HER2. This marker combination has been shown to effectively differentiate cancer from host cells (*13*, *31*, *32*). We observed a good correlation between expected and measured cancer cell counts in mixtures of cancer and immune cells (T or B cells) with varying cell proportions (Pearson correlation coefficient $r = 0.95$, $P = 0.0042$; fig. S2). The detected malignant cells were subsequently classified into four subtypes based on ER, PR, and HER2 status: luminal HER2 negative $(ER/PR)^+(HER2)^-$, luminal HER2 positive $(ER/PR)^+(HER2)^+$, HER2 positive $(ER/PR)^-(HER2)^+$, and triple negative $(ER/PR)^-(HER2)^-$ (fig. S3). Such classification is clinically important because it can guide choosing the most appropriate treatment (*33*). For example, ER/PR-positive patients would benefit from therapy with selective ER modulator (such as tamoxifen), antiestrogen (such as fulvestrant), or aromatase inhibitors. Similarly, HER2-positive patients would benefit from anti-HER2 treatment (such as trastuzumab).

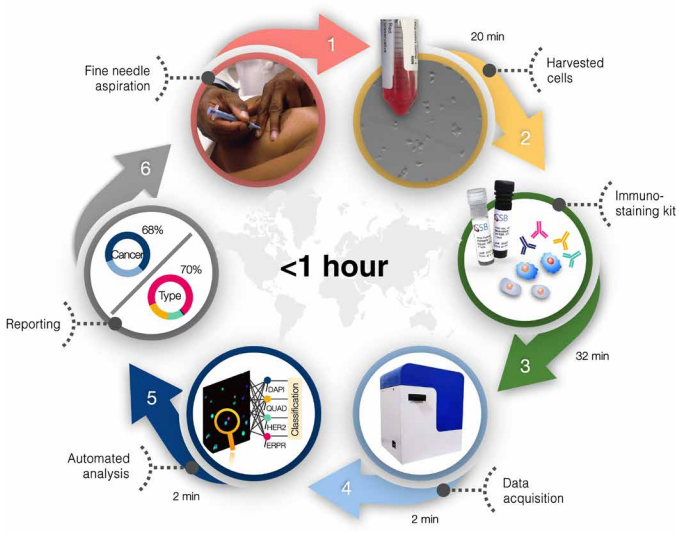

Fig. 1. Schematic of the CytoPAN workflow. Step 1: Cellular samples are obtained from patients with breast cancer via fine needle aspiration. Step 2: The harvested cells are briefly fixed and semipermeabilized. Step 3: Samples are processed with prefabricated lyophilized kits containing all necessary antibodies for breast cancer diagnosis, including ER, PR, HER2, and Quad. Step 4: The stained cells are analyzed by the CytoPAN device. Step 5: For fast and automated data analysis, custom-developed algorithms are applied to identify cancer cells, separate them from host cells, and extract their marker information. Step 6: A final diagnostic report displays a set of quantitative information, including the cancer cell population and molecular subtype distribution in a patient sample. Depending on initial results, a repeat biopsy could be taken within an hour should the sample be nondiagnostic. Step 1 is adapted from National Cancer Institute (https://visualsonline.cancer.gov/details.cfm?imageid=1973).

Assay optimization

Field testing requires a simple assay protocol. We thus optimized assays to satisfy the following criteria: (i) few steps for labeling and washing, (ii) fast (within 1 hour), and (iii) high signal-to-background ratios. We specifically tested different fixation, permeabilization, blocking, staining, and washing conditions. As a model system, we used established breast cancer cell lines, namely, BT474 $(ER/PR)^+(HER2)^+$ and MCF7 $(ER/PR)^+(HER2)^-$ as receptor-positive cell types and MDA-MB-231 $(ER/PR)^-(HER2)^-$ as a receptor-negative, namely, triple-negative breast cancer (TNBC) cell type.

We first surveyed the fixation method for FNA specimens. Among various fixatives available (for example, BD Lyse/Fix, alcohol, and paraformaldehyde), the ideal fixative for clinical FNA samples should (i) fix the cells, (ii) lyse red blood cells (RBCs), and (iii) preserve antigens during sample transfer to laboratories (from a few hours up to a day at room temperature). Considering these factors, we chose CytoRich Red (CRR), a fixative commonly used in cytology. CRR is a formalin-based fixative solution that lyses RBCs and solubilizes proteins. We identified the optimal fixation protocol

to be 15-min incubation in CRR, which showed high signals and sensitivity comparable to paraformaldehyde-based fixation (fig. S4). After 1 day of storage at room temperature, FNA specimens in CRR solution still had/demonstrated high signal-to-background ratios. By contrast, longer fixation with paraformaldehyde at room temperature tends to increase cellular autofluorescence (*34*, *35*). After fixation, cells were permeabilized to enable the detection of intracellular proteins (ER/PR). The use of Triton X-100 for permeabilization after fixation is common, but we found it excessively harsh on cell membranes to the extent of lowering HER2 and Quad signals (fig. S5). A milder permeabilization method with saponin-based buffer (BD perm) showed better signal-to-noise ratios for both membrane (Quad and HER2) and intracellular proteins (ER/PR).

Next, we optimized sample preparation and immunostaining time (Fig. 2A). A direct staining method, which requires only one labeling step, was preferable because of its simplicity, but intracellular protein (ER/PR) signals were low with this method (fig. S6). Instead, we chose a primary/secondary labeling approach and tested varying incubation/washing times. We used a cocktail of antibodies for primary and secondary immunostaining to further reduce assay time and determine optimal antibody concentrations. Among several conditions tested, the finalized protocol consisted of permeabilization (10 min), blocking (10 min), primary antibody staining (20 min) followed by 1-min washing, and secondary antibody staining (10 min) followed by 1-min washing. This procedure (condition no. 4 in Fig. 2A) showed the highest signal-to-noise ratio and high sensitivity for both HER2 and ER/PR while maintaining assay times under 1 hour (Fig. 2B).

Last, to test the assay under more stringent environmental conditions, such as those found in many LMICs, we lyophilized antibody cocktails and tested different storage conditions (−20°, 4°, and 20°C). We observed overall signal decrease (~25%) when lyophilized antibodies were used; this could be attributed to the physical loss of antibodies from the buffer exchange step and/or conformational changes from shearing during the freeze-drying step (*36*). To compensate for the signal loss, we increased the initial amount of antibodies by 25%, which restored analytical signals to levels comparable with those from fresh nonlyophilized antibodies (Fig. 2C). The lyophilized antibodies could be stored at different temperatures (−20°C for long-term storage and 4° or 20°C for short-term storage) without notable proteolytic degradation (Fig. 2D and fig. S7).

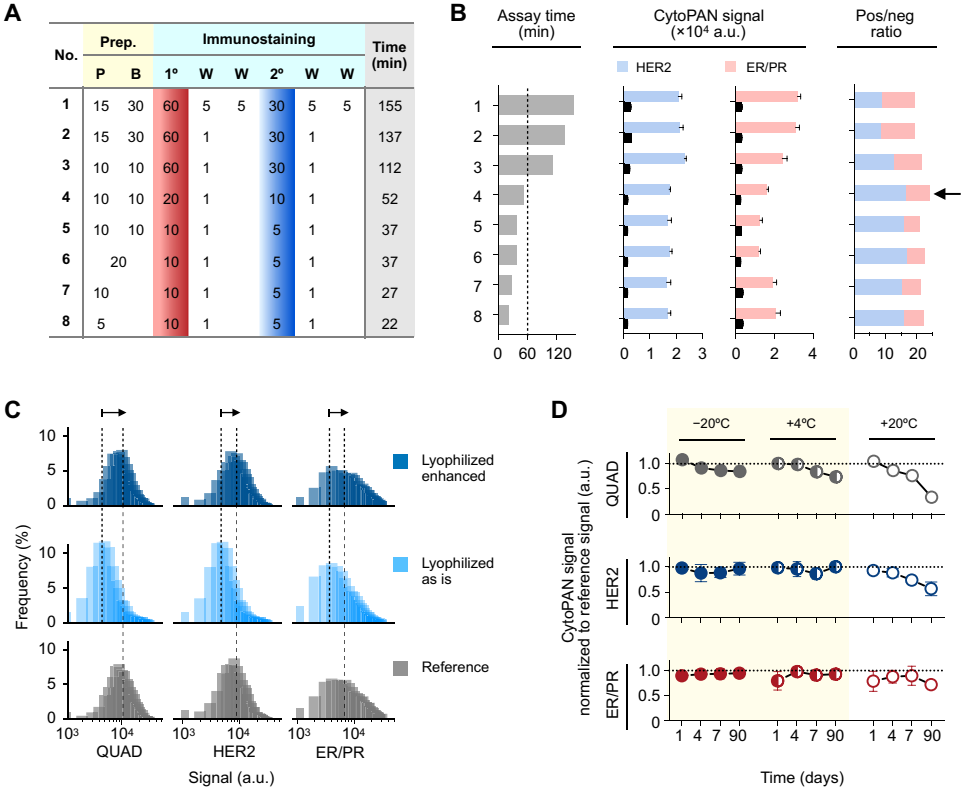

Fig. 2. Assay optimization. (**A**) Different assay protocols were tested to determine which optimally satisfies all of the following criteria: (i) fast (less than 1 hour), (ii) simple (few steps for labeling and washing), (iii) detects signals above threshold values, and (iv) high sensitivity. P, permeabilization; B, blocking; W, washing; 1°, primary antibody staining; 2°, secondary antibody staining. (**B**) Among the eight protocols tested, we identified no. 4 as the best, showing high signal and sensitivity for both intracellular and surface target markers while maintaining the assay time below 1 hour. a.u., arbitrary units; Pos/neg, positive/negative. (**C**) We compared the performance of lyophilized antibodies, with (lyophilized enhanced) or without (lyophilized as is) adjusting the antibody concentrations by 20 to 30%, to that of the fresh nonlyophilized ones (references). (**D**) Stability of lyophilized antibody cocktails stored at different temperatures (−20°, 4°, and 20°C) was assessed over different periods of time. All data were displayed as means ± SD ($n = 3$). Dotted lines indicate reference value.

System design and performance

We designed the CytoPAN device hardware to offer a compact, cost-effective system for multiplexed cellular analysis (Fig. 3A). The device was equipped with multiple light sources for five optical channels: bright-field and four fluorescence imaging (excitation wavelengths at 365, 405, 488, and 638 nm). We used a white light-emitting diode (LED) for bright-field flood illumination, an LED (365 nm) and laser diodes (405, 488, and 638 nm) for fluorescence excitation (table S1). Key components of the design included excitation light sources positioned on the sample plane for side illumination and a quad bandpass filter. In this configuration, the excitation light did not directly illuminate an image sensor, eliminating the need for excitation filters or dichroic mirrors and therefore reducing the space outline. Furthermore, the single quad bandpass filter blocked excitation light but transmitted emission light through four bandpass wavelength zones. This eliminated the use of multiple filter sets with mechanical actuation and improved operational efficiency and system stability. The relative fluorophore contributions between channels were measured to characterize bleed-through and cross talk (fig. S8). On the basis of the measured values, we performed a mathematical correction of signal overlap between channels to

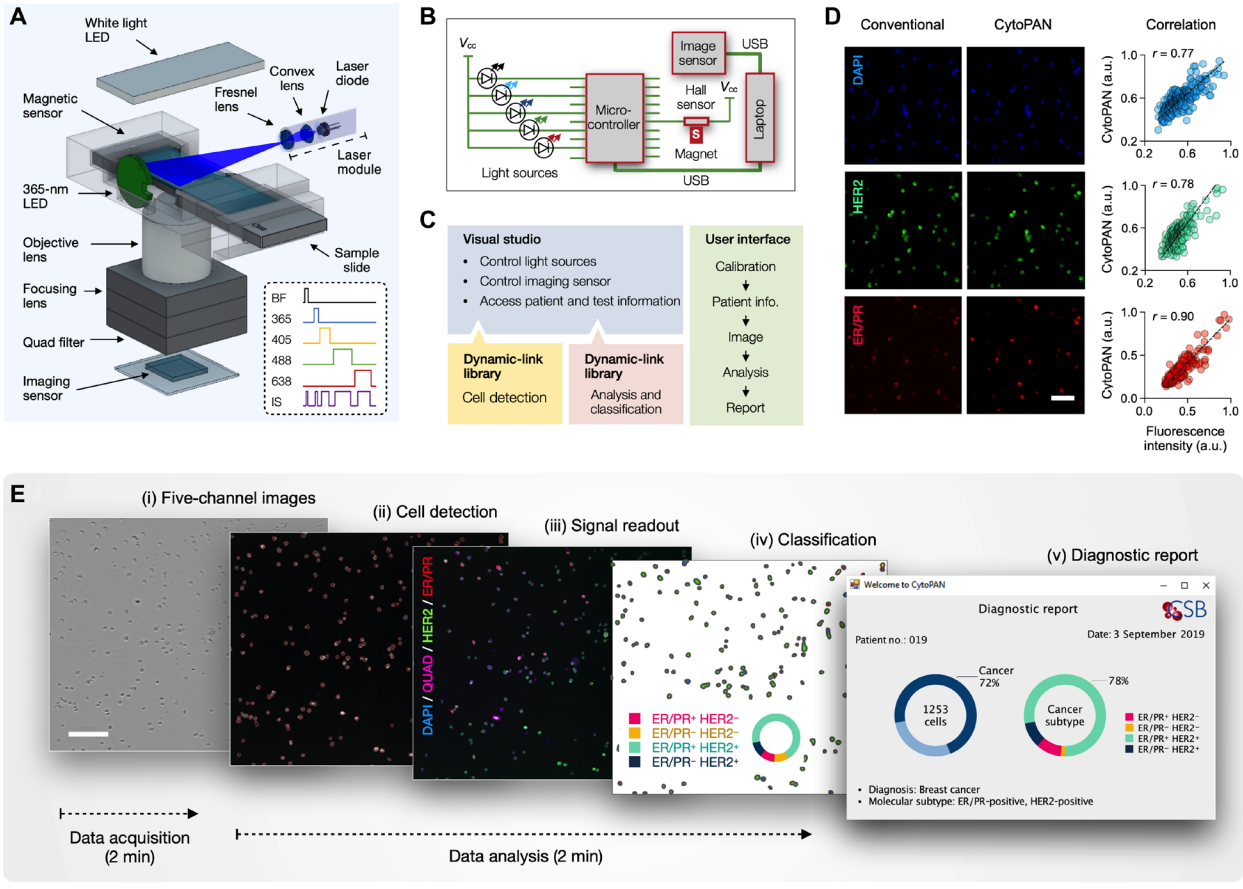

Fig. 3. CytoPAN device and data analysis. (**A**) Schematic of the CytoPAN system, which consists of light sources, an optical imaging module, and a customized sample holder with a Hall sensor as a positioning switch. (**B**) The light sources and Hall effect sensor are controlled by a microcontroller, which, along with an imaging sensor, is universal serial bus (USB)–connected to a personal computer. (**C**) A software package was developed to check the system calibration and status, control the light sources and imaging sensor, and monitor and analyze data. A user-friendly interface was designed for fast user learning and seamless system operation. (**D**) Measurements of DAPI, HER2, and ER/PR signals of BT474 cells showed good correlations between the CytoPAN and a conventional microscope ($r = 0.77$, $P < 0.0001$ for DAPI; $r = 0.78$, $P < 0.0001$ for HER2; $r = 0.90$, $P < 0.0001$ for ER/PR). Scale bar, 100 μm. (**E**) Automated data analysis workflow: (i) capture five-channel images; (ii) use bright-field and DAPI images for cell segmentation; (iii) among detected cells, identify malignant cells based on Quad signals; (iv) color-code cancer subtypes based on ER/PR and HER positivity; and (v) display a final diagnostic report. The data acquisition/analysis process takes only 4 min. Scale bar, 200 μm.

minimize false-positive signals. Our results showed that this correction accurately reflected true biomarker signals (fig. S8) and was similar to the corrections implemented on most commercial cytometers.

Images were recorded by a monochrome image sensor (5 megapixels, pixel size of 3.45 μm) with a field of view of 1.2 mm by 1.4 mm. The system used a Hall sensor to detect a small magnet embedded in the sample holder; this magnetic interlock assisted in sample positioning and prevented from reading of "slides" without samples present. We programmed a microcontroller to synchronize imaging operations by sequentially turning light sources on and off and triggering image acquisition (Fig. 3B). All five-channel images were automatically acquired within 30 s and transferred to a computer for analysis. We also developed a graphical interface to guide end users for system calibration, imaging, and analysis (Fig. 3C and fig. S9). The simple, intuitive user interface would facilitate user learning and efficient system operation. The system had a small form factor (20 cm by 20 cm by 28 cm), and component costs were about $3500 (table S2). Component costs could decrease to ~$1500 through economies of scale and substituting for lower-cost alternative components.

We next benchmarked the CytoPAN device against a conventional (~$200,000) upright fluorescence microscope (Olympus BX63 equipped with an Andor Neo camera). We used fluorescence calibration beads (6 μm in diameter) and the triple-positive cell line (BT474) for system characterization. The CytoPAN produced high-quality images with high signal-to-noise and signal-to-background ratios highly comparable to those acquired by the commercial microscope (Fig. 3D and fig. S10). The fluorescence signal of individual cells measured by the CytoPAN and the conventional microscope showed good correlations for all channels tested ($P < 0.0001$; Fig. 3D). To evaluate the reproducibility of the CytoPAN system, we also imaged the stained BT474 cells over different days. The normalized intensities had an interdaily coefficient of variation of <3% (fig. S10C).

Figure 3E shows the automated workflow of CytoPAN analysis: (i) Five-channel images are acquired; (ii) bright-field and 4′,6-diamidino-2-phenylindole (DAPI) images are used for cell segmentation; (iii) malignant cells are identified on the basis of the Quad signals; (iv) subtypes are color-coded on the basis of ER/PR and HER expressions; and (v) reported end results include quantitative

readouts of malignant cell counts and cell proportions among subtypes. The analysis of ~10^3 cells is completed within 2 min, and a final diagnostic report is displayed on the interface.

Assay validation

We next applied CytoPAN to profile a panel of breast cancer cell lines that have different molecular phenotypes: MCF7 and T47D, $(ER/PR)^+(HER2)^-$; BT474, $(ER/PR)^+(HER2)^+$; SkBr3 and HCC1954, $(ER/PR)^-(HER2)^+$; MDA-MB-231 and HCC1937, $(ER/PR)^-(HER2)^-$. Cells were fluorescently labeled with DAPI (365-nm channel) or for Quad (405 nm), HER2 (488 nm), and ER/PR (638 nm); control samples were labeled with isotype-matched immunoglobulin G (IgG) antibodies. The cutoff levels for marker positivity were set as a mean intensity of +2 × SD of control IgG samples. The scatter plots (Fig. 4A) show successfully identified cellular subtypes. As expected, the triple-positive cell line (BT474) showed positive signals for both ER/PR and HER2 expressions, whereas the triple-negative cell line (MDA-MB-231) showed negative signals. In the case of MCF7, ER/PR signals were high, whereas HER2 signals were dominant in HCC1954. The CytoPAN results were also consistent with those obtained by flow cytometry; the proportion of each cell type positive for markers was well matched between two systems (fig. S11). We also observed excellent correlations ($r > 0.97$) between the mean signals of target markers, highlighting the accuracy of the CytoPAN system (Fig. 4B). The more compact CytoPAN, however, excelled in accessibility: It required much smaller sample volumes than a conventional flow cytometer and enabled portable operation.

Analyzing mouse models of breast cancer

We next set out to analyze FNA samples obtained from mouse xenografts. These studies were performed to optimize and validate the cutoff values for marker positivity and confirm that repeat biopsies resulted in congruent data. Mice typically underwent two to five FNA passes when tumors had grown to about 5 to 7 mm in diameter (Fig. 5A). We used four cell lines that represent the spectrum of human breast cancer subtypes: MCF7, BT474, HCC1954, and MDA-MB-231 (Fig. 5B). The average number of cells obtained from a single 22-gauge needle pass is modest (~10^4 cells on average) but sufficient to perform the CytoPAN assay. Cells were immunostained against the five target markers, and their fluorescence signals were recorded by the CytoPAN system (Fig. 5C). For each FNA sample, we determined total cell counts, cell size, and marker-positive cell counts (Fig. 5D). The results showed that (i) FNA can be obtained in small mouse tumors, yielding a sufficient number of cells for analysis; (ii) harvested cells included both cancer cells and host cells, which could be differentiated by marker and size analysis; (iii) FNA allowed correct molecular subtyping of breast cancers; and (iv) repeat FNA on different days resulted in similar diagnoses, which demonstrated the reproducibility of measurements (Fig. 5E). Furthermore, the automated CytoPAN was able to complete the multiplexed analysis of hundreds of cells within minutes without the need for high-end computing power, and the results matched well with flow cytometry reports when more cells were harvested for the latter (fig. S12).

Clinical testing in FNA

To determine the clinical utility of the approach, we next conducted a prospective clinical study in which the FNA could be directly compared to conventional pathology results. We enrolled treatment-native patients at the Kyungpook National University Chilgok Hospital (Daegu, South Korea) and who were referred for primary surgery. All patients consented to have a preoperative breast FNA before

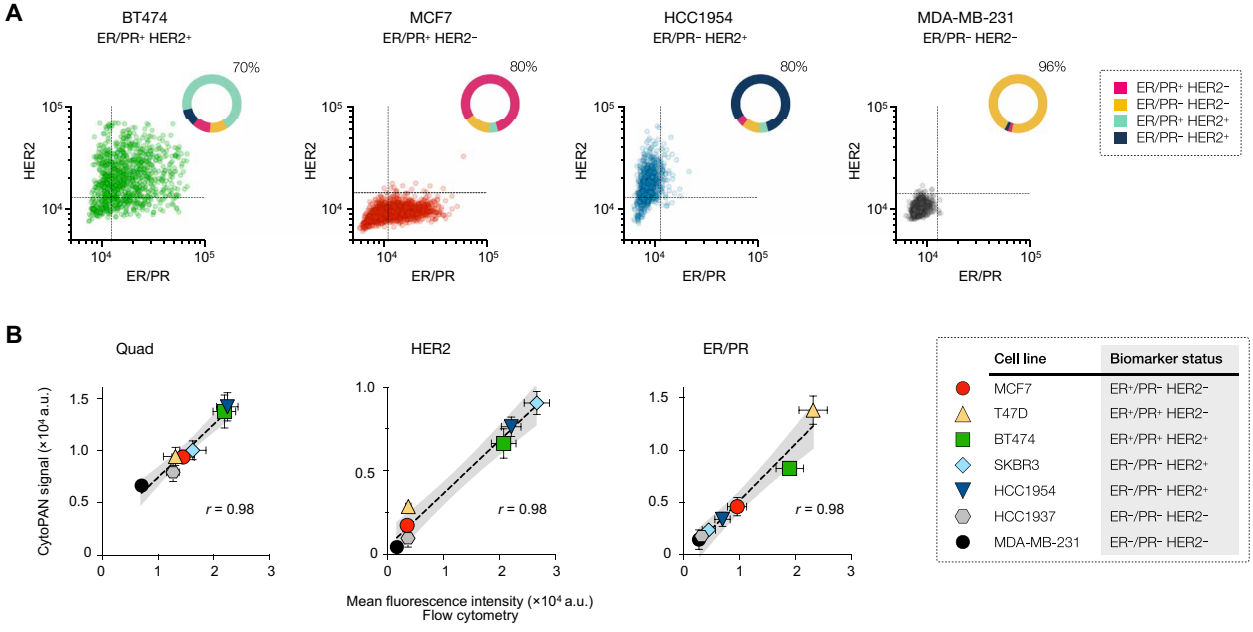

Fig. 4. Validation against gold standards using cell lines. (**A**) Breast cancer cell lines representing four subtypes [MDA-MB-231, $(ER/PR)^-(HER2)^-$; BT474, $(ER/PR)^+(HER2)^+$; HCC1954, $(ER/PR)^-(HER2)^+$; MCF7, $(ER/PR)^+(HER2)^-$] were immunolabeled against Quad, ER/PR, and HER2 and then profiled using the CytoPAN device. More than 500 individual cells were analyzed for each subtype. Dashed lines indicate positive cutoffs for ER/PR and HER2. (**B**) Correlation between CytoPAN and flow cytometry measurements of target biomarkers in various breast cancer cell lines ($r = 0.98$, $P = 0.0002$ for Quad; $r = 0.98$, $P < 0.0001$ for HER2; $r = 0.99$, $P < 0.0001$ for ER/PR). At least 100 individual cells were analyzed for CytoPAN and >8000 cells for flow cytometry, and all data were presented as means ± SD ($n = 3$). The linear least squares fitting was performed at the 95% confidence level.

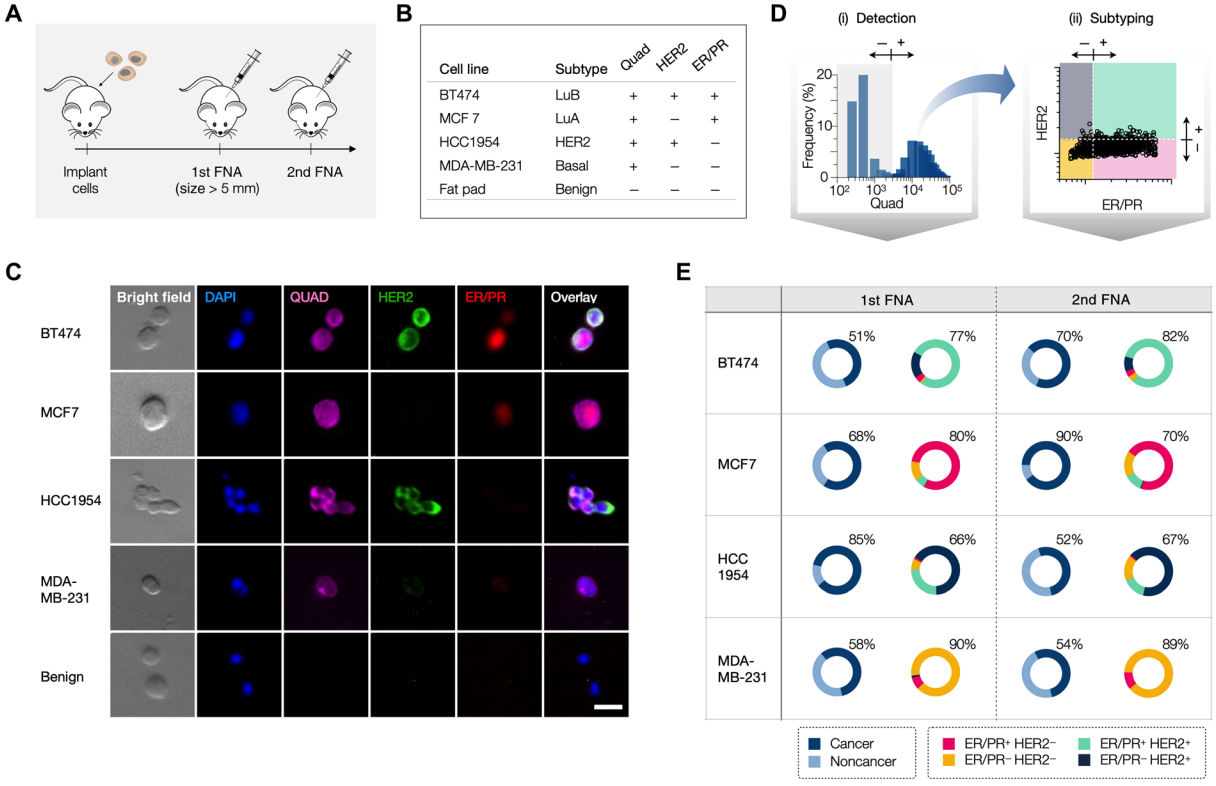

Fig. 5. In vivo studies using human breast cancer xenograft models. (**A**) Schematic representation of the FNA protocol in mice. (**B**) Breast cancer cell types in the mouse xenograft models representing four subtypes [MDA-MB-231, (ER/PR)$^-$(HER2)$^-$; BT474, (ER/PR)$^+$(HER2)$^+$; HCC1954, (ER/PR)$^-$(HER2)$^+$; MCF7, (ER/PR)$^+$(HER2)$^-$]. (**C**) Representative raw images of different FNA specimens taken by the CytoPAN device for bright field, DAPI (blue), Quad (magenta), HER2 (green), ER/PR (red), and overlay. Scale bar, 20 μm. (**D**) Algorithms for (i) malignant/normal cell differentiation and (ii) breast cancer subtype classification. (**E**) Diagnostic results are consistent for repeat FNA collected at different time points, indicating assay repeatability and robustness.

clinically indicated surgery. The breast masses were visualized by ultrasound or computed tomography, and a coaxial needle was introduced through which FNA samples (CytoPAN) and core biopsies were obtained. Surgical specimens and/or core biopsies were processed by routine pathology and served as the gold standard. All samples were processed in a blinded format until the end of the study. All samples were processed as described above for the mouse co-clinical trial and using the previously established algorithm and cutoffs (Fig. 6A and fig. S13). Of the 68 patients enrolled, we found sufficient numbers of harvested cells in 63 patients (93%). The remaining five samples (7%) were deemed nondiagnostic because they contained <50 cells. The algorithm further determined tumor/host cell composition by (i) Quad marker positivity, (ii) cell size (cutoff diameter of ~8 μm), and (iii) CD45 staining as illustrated in Fig. 6A and fig. S14.

Figure 6B shows representative examples of analyses obtained from five representative patients, four with different types of breast cancer and one with a benign mass. As can be seen, results obtained by FNA-CytoPAN yield cell numbers in the thousands and allow automated scoring of host and cancer cell population. Furthermore, image analysis on single cells allows rapid receptor typing leading to percentage and categorical diagnoses. For example, patient no. 58 was diagnosed as benign, whereas patient nos. 20, 25, 5, and 37 had invasive breast cancer with high Quad expression. Patient no. 20 showed high ER/PR (99%) but low HER2 (1%) expression, whereas patient no. 25 exhibited low expression of ER/PR (13%) and high HER2 (53%). Patient no. 5 was diagnosed with triple-positive breast cancer, and patient no. 37 was diagnosed with TNBC with low ER/PR (1%) and low HER2 (0%).

Table 1 summarizes the detailed data from all 68 patients enrolled in the study, and Fig. 7 shows the data and their analyses. For the 63 patients in whom sufficient cells were present, we analyzed a mean of 1308 (range, 93 to 11,985) cells per patient. Fifty-five patients had malignant breast cancer, and five patients had benign lesions as correctly determined by CytoPAN analysis (Fig. 7A). Three cases were inconclusive because of low number of Quad-positive cells for further analysis. Furthermore, CytoPAN analysis allowed receptor typing in all patients (Fig. 7B). Using receiver operating characteristic (ROC) analyses, we determined sensitivity, specificity, and the area under the curve (AUC; Fig. 7C). The diagnostic accuracy for deterring cancer was 100%. The diagnostic accuracy for receptor subtyping was 93% for ER/PR (51/55) and 96% for HER2 (53/55).

The specimens from two patients (patient nos. 30 and 34) showed false-positive CytoPAN results for HER2 subtyping, but it should be noted that both patients only had a pathology/immunohistochemistry (IHC) score of 2 ("equivocal/intermediate"). With respect to ER/PR subtyping, the specimens from four patients (patient nos. 3, 50, 52, and 62) showed false-negative results. This discrepancy could be attributed to the following causes: (i) equivocal ER/PR expression and cutoffs by IHC (patient no. 50 showed 4% ER/PR positivity by CytoPAN and 10% ER positivity and 2% PR positivity by IHC) and (ii) discordant biopsy of different areas within a tumor, but less

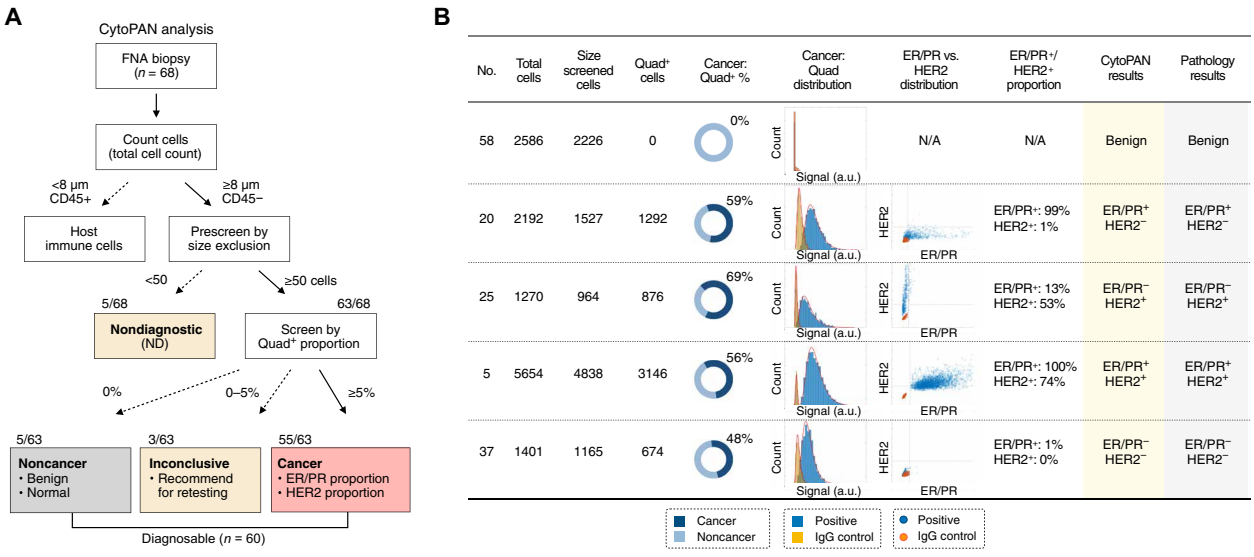

Fig. 6. CytoPAN analysis of human breast FNA. (**A**) Diagnostic algorithm applied to clinical validation cohort. Detected cells were first prescreened by size exclusion (>8 μm). If fewer than 50 Quad-positive cells were present, we deemed the sample nondiagnostic. Above that number, we classified the specimen as malignant, benign, or inconclusive depending on the prevalence of Quad-positive cells in the sample. (**B**) Five representative examples of CytoPAN analyses are shown (four malignant and one benign; see Table 1 for results from all 68 patients). For all four malignant samples, there was good agreement between surgical pathology (IHC) and CytoPAN analysis. Note the number of cells analyzed in this subset analysis.

likely technical reasons, because all quality control test results were within normal limits.

DISCUSSION

Several detection technologies have the potential to be developed into affordable, POC versions for use in resource-limited settings (*37*–*39*). In practice, however, the number of viable technologies is much smaller, given the constraints of cost, accuracy, complexity, and practicality in resource-limited settings. There are two major prerequisites that have received less attention: (i) For fast processing and low morbidity, sample analysis ideally relies on harvested cells rather than tissue, and (ii) a given assay must be multiplexable to assess biomarker panels in all cells (as opposed to aliquoting samples for separate measurements). These criteria underpin the current work and largely arose from lessons learned during field testing of prior technological approaches (*17*, *18*).

We engineered an integrated image cytometry platform to enable same-day diagnosis and treatment of breast lesions. The CytoPAN system is self-contained and can potentially be operated by nonphysicians after brief training. The approach addresses the huge need of providing broader POC diagnosis and faster turnarounds than are possible in many settings (*40*). Apart from the current trial reported here, the system is also being deployed in field trials in Botswana (NIH UH3CA202637). The ultimate outcome of these LMIC studies will require some time to establish as only a small fraction of patients to date were able to receive pathology reports due to limited medical infrastructure for surgical core biopsy, delayed pathology workup, and/or loss of patient follow-up.

Cancer specimens are commonly obtained by image-guided tissue biopsy, surgical tissue harvesting, punch biopsies, brushings, swabs, touch preps, fluid aspiration, or blood analyses (leukemia, lymphoma, and liquid biopsies). Some of these methods (core and open surgical biopsies) yield abundant tissue for embedding, sectioning, and staining for subsequent histopathological analysis. Although well established, this workflow is lengthy and requires expensive instrumentation and a trained workforce. In contrast, FNAs can be performed with minimal intervention using much smaller-gauge needles (20 to 25 gauge), have very low complication rates, and are generally well tolerated (*29*, *41*). Unfortunately, FNA of solid neoplasms typically yields scant cellular material, often challenging conventional analyses with colorimetric staining, IHC, and expert cytopathological review.

Given the paucity of cells in FNA, there is a need to extract as much information as possible from each harvested cell. This need dictates the use of multiplexed assays, particularly methods that are inexpensive, simple, and robust. For LMIC use, these requirements make fluorescence optical imaging a primary choice, because biomarkers of interest can be assigned to different fluorescence channels. Conventional cytopathology generally relies on chromogenic immunostaining to better define cellular morphology, but this requires expert analysis. We found fluorescence staining more ideally suited to automated analysis, similar to flow cytometry. Another key advantage of the CytoPAN is the minimum number of cells required for diagnosis (>50 cells). Given the well-established and documented variation in the number of cells collected by FNA (~10^2 to 10^6), the CytoPAN would be preferred over flow cytometry for FNA analysis. In our current work, we combined five channels into a single device without any moving parts. This was performed by implementing a quad filter and side illumination into a bare bones system. In the future, it may be possible to extend the multiplexing capabilities from 5 to 40 to 60 markers by harnessing image cycling approaches for FNA (*42*, *43*).

One of the key design elements in the current system is lyophilized kits containing all necessary antibodies, buffers, and other reactants. A similar approach had previously been realized for lymphoma (*44*) but nevertheless required reanalysis for breast cancer because it required us to target different markers. Major advantages of these freeze-dried kits include (i) expanding the shelf life of kits

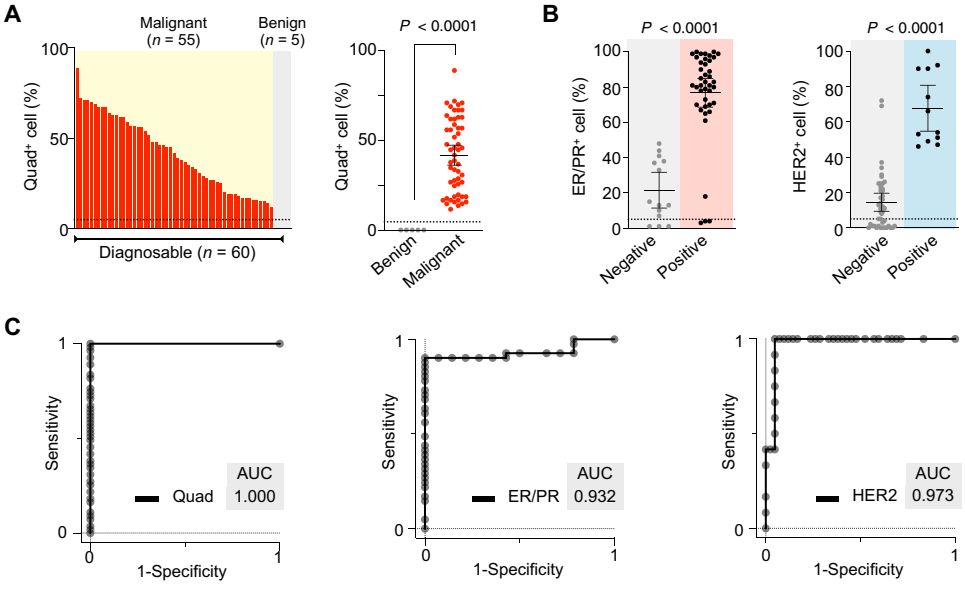

Fig. 7. Cancer diagnosis analysis. (**A**) A waterfall plot shows the Quad-positive cell population prevalence sorted from high (left) to low (right) for 60 diagnosable samples (55 malignant and 5 benign tumors). Each column represents a different patient sample. There were no Quad-positive cells in benign samples. The Quad signature showed 100% accuracy in distinguishing malignant from benign samples ($P < 0.0001$, unpaired t test). (**B**) The ER/PR-positive and the HER2-positive population prevalence were measured for 55 malignant samples ($P < 0.0001$, unpaired t test). (**C**) ROC curves were calculated for target markers (Quad, ER/PR, and HER2) with optimum threshold values. AUC, area under the curve.

from hours to weeks or months, a critical factor for field testing; (ii) enabling storage in regular refrigerators rather than specialty freezers commonly unavailable in LMICs; (iii) more efficient use of expensive specialty reagents; (iv) simplification of multistep procedures so that they can be performed by a less skilled workforce; and (v) reduction in assay cost. Through judicious choice of lyophilization conditions, we found that (i) antibody performance can be improved by increasing the initial amount of antibodies by 25% to compensate for the loss of activity and (ii) the functionality of the lyophilized antibodies could be maintained over 90 days if stored at or below 4°C.

The estimated cost for each test kit is under $5, more than five times lower than the current cost of conducting diagnostic pathology tests. The costs per histopathology slide are $149 in Lilongwe and $24 to 28 in Nebraska (*45*). Note that the estimated cost per slide in Nebraska does not include time and cost for pathologist's review and interpretation. In addition, the cost efficiencies generated by our approach stem from the improved accuracy via automated, operator-free imaging analysis (less subjectivity), increased throughput from faster turnaround times, and increased productivity (more efficient use of human capital) among other factors.

An essential part of the technology development was complete automation of image acquisition, built-in quality control routines, and operator-independent analysis. To minimize variations in fluorescence intensities between experiments and on different days, we implemented bead-based calibration routines before each experiment in all four fluorescence channels. We devised serial wide-field image acquisitions by programming imaging routines in bright-field, DAPI, Quad, HER2, and ER/PR channels. We applied custom-developed automatic analysis algorithms for cell segmentation, expression level thresholding, and cellular analysis. Each of these routines was essential in proving automated operation without user curation. We also implemented several additional safeguards. Users could only proceed with image acquisition when the program detected the microcontroller and the imaging sensors were connected and switched on. To prevent triggering image acquisition without a sample in place, we installed a magnetic interlock that detected the proper positioning of a sample slide.

In the current study, we first optimized and validated technical aspects in cell lines and a mouse co-clinical trial. This allowed us to carefully investigate individual parameters, establish cutoff values, and confirm that repeat biopsies produced congruent data. The different thresholds and controls were then corroborated in a prospective clinical trial using conventional histopathology as the gold standard. To assure correct diagnoses and avoid over and under treatments, appropriate quality controls are essential. In our case, this included operator training and recertification in FNA sampling and operational quality controls (see Materials and Methods). In borderline cases, the sample materials were generally scant and were flagged as such.

In the clinical cohort, we showed a high rate of diagnosable FNA samples (93%). This number compares favorably with biopsy results in developed countries, where up to ~20% of samples are deemed "nondiagnostic" (*46*). In the 63 samples with adequate cellular materials, there was good correlation with histopathology. For a cancer diagnosis, the observed diagnostic accuracy was 100% (false-positive rate, 0%; false-negative rate, 0%). The receptor subtopic accuracy was 96% for HER2 and 93% for ER/PR.

The results are notable in several aspects. First, each sample underwent a full processing cycle in only 1 hour. Second, we were able to establish accurate cancer diagnoses with as few as 50 cancer cells analyzed per specimen. This is especially important because not all FNAs are equally cellularly rich, particularly when only single passes are obtained (patient or cultural preferences) or inexperienced users take samples (*47*). Last, we determined that reliable receptor subtyping also required very few cancer cells. That is, accurate cancer diagnosis should be possible with cells from single FNA passes.

The current study had some limitations as the main goal was to develop, optimize, and validate an FNA analysis system that could be used for global and remote applications. First, the patient population studied (treatment-naive surgical candidates without other major comorbidities) may not be representative of that in LMIC. For example, it is estimated that in sub-Saharan Africa, 20 to 40% of women diagnosed with breast cancer will be HIV positive (*48*–*50*). Conversely, in developed countries, a large portion of suspicious lesions are detected by mammography rather than by manual palpation. On the basis of these observations, we envision future prospective clinical trials in different remote and U.S. locations. Second, the number of molecular biomarkers used in this study was kept to a minimum for logistical and cost reasons in LMIC. With further modifications, it is feasible to expand the number of channels or use

Table 1. Summary of clinical results. Results for 68 patients who had both FNA and core biopsies of breast masses. Fifty-eight of the masses were malignant, and 10 mass were benign. Five FNA sample were nondiagnostic as it only contained less than 50 cells, and three were inconclusive. Note the excellent match between the different analyses (1-hour automated cellular analysis versus conventional surgical pathology analysis, which takes several days. For CytoPAN, Total, $DAPI^+$; cancer, $DAPI^+$ $Size^+$ $QUAD^+$; Quad (%) = cancer/screened; ER/PR (%) = ER/PR^+/cancer; HER2 (%) = $HER2^+$/cancer. For pathology, ER/PR score, proportion score (0 to 5) + intensity score (0 to 3); HER2 score, 0 to 1 (negative), 2 (equivocal), and 3 (positive).

	CytoPAN (1 hour; scant cells)									Pathology (days; core immunohistochemistry)								
No.	Total count	Cancer: Quad (%)	ER/PR^+ (%)	$HER2^+$ (%)	Cancer dx	Sub type dx	Quad match	ER/PR match	HER2 match	Cancer dx	Sub type dx	ER/PR^+ status	HER^+ status	ER score	ER (%)	PR score	PR (%)	HER2 score
1	661	0.16	0.73	0	1	ER/PR+	O	O	O	1	ER/PR^+	1	0	5+3=8	95	5+3=8	95	1
2	2500	0.45	0.81	1	1	TP	O	O	O	1	TP	1	1	5+3=8	95	3+3=6	25	3
3	682	0.19	0.18	0.01	1	TN	O	X	O	1	ER/PR^+	1	0	4+2=6	40	5+3=8	95	2
4	441	0.15	1	0.25	1	ER/PR^+	O	O	O	1	ER/PR^+	1	0	5+3=8	95	0+0=0	0	1
5	5654	0.56	1	0.74	1	TP	O	O	O	1	TP	1	1	5+3=8	98	4+3=7	60	3
6	1234	0.33	0.95	0.21	1	ER/PR^+	O	O	O	1	ER/PR^+	1	0	5+3=8	95	4+2=6	50	1
7	610	0.62	0.1	0.11	1	TN	O	O	O	1	TN	0	0	0+0=0	0	0+0=0	0	1
8	11,985	0.37	0.97	0.18	1	ER/PR^+	O	O	O	1	ER/PR^+	1	0	5+3=8	98	3+3=6	40	1
9	684	0.02	–	–	***Repeat***					1	ER/PR^+	1	0	5+3=8	95	5+3=8	95	2
10	3037	0.72	0.7	0.25	1	ER/PR^+	O	O	O	1	ER/PR^+	1	0	5+3=8	90	4+3=7	60	0
11	305	0.28	0.15	0.23	1	TN	O	O	O	1	TN	0	0	2+2=4	10	0+0=0	0	0
12	992	0.71	0.81	0.9	1	TP	O	O	O	1	TP	1	1	5+3=8	90	5+3=8	90	3
13	415	0.27	0.98	0	1	ER/PR^+	O	O	O	1	ER/PR^+	1	0	5+3=8	98	5+3=8	85	1
14	489	0.38	0.93	0.09	1	ER/PR^+	O	O	O	1	ER/PR^+	1	0	5+3=8	95	5+2=7	85	2
15	3	0	–	–	***ND***					1	ER/PR^+	1	0	5+3=8	95	5+3=8	90	1
16	786	0.57	0.66	0.01	1	ER/PR^+	O	O	O	1	ER/PR^+	1	0	5+3=8	95	3+2=5	25	1
17	2106	0.39	0.83	0.04	1	ER/PR^+	O	O	O	1	ER/PR^+	1	0	0+0=0	0	0+0=0	0	1
18	4426	0.64	0.44	0.54	1	$HER2^+$	O	O	O	1	$HER2^+$	0	1	0+0=0	0	0+0=0	0	3
19	1901	0.2	0.37	0.66	1	$HER2^+$	O	O	O	1	$HER2^+$	0	1	2+1=3	5	0+0=0	0	3
20	2192	0.59	0.99	0.01	1	ER/PR^+	O	O	O	1	ER/PR^+	1	0	5+2=7	95	5+3=8	80	1
21	1247	0.63	0.99	0.01	1	ER/PR^+	O	O	O	1	ER/PR^+	1	0	5+3=8	98	5+3=8	90	1
22	34	0.12	–	–	***ND***					0		–	–	–	–	–	–	–
23	1421	0.67	0.9	0.21	1	ER/PR^+	O	O	O	1	ER/PR^+	1	0	5+3=8	98	5+3=8	98	1
24	508	0.56	0.07	0.13	1	TN	O	O	O	1	TN	0	0	0+0=0	0	0+0=0	0	1
25	1270	0.69	0.13	0.53	1	$HER2^+$	O	O	O	1	$HER2^+$	0	1	2+2=4	5	2+1=3	5	3
26	217	0.34	0.38	0	1	TN	O	O	O	1	TN	0	0	0+0=0	0	0+0=0	0	0
27	268	0.46	0.8	0.12	1	ER/PR^+	O	O	O	1	ER/PR^+	1	0	5+3=8		0+0=0	0	0
28	583	0.62	0.99	0.01	1	ER/PR^+	O	O	O	1	ER/PR^+	1	0	5+3=8	98	5+3=8	98	2
29	795	0.46	0.01	0	1	TN	O	O	O	1	TN	0	0	2+3=5	10	0+0=0	0	1
30	1893	0.57	0.33	0.72	1	$HER2^+$	O	O	X	1	TN	0	0	0+0=0	0	0+0=0	0	2
31	1029	0.48	0.69	0.11	1	ER/PR^+	O	O	O	1	ER/PR^+	1	0	5+3=8	95	5+3=8	90	1
32	993	0.18	0.48	0.92	1	$HER2^+$	O	O	O	1	$HER2^+$	0	1	0+0=0	0	0+0=0	0	3
33	2618	0.45	0.99	0.37	1	ER/PR^+	O	O	O	1	ER/PR^+	1	0	5+2=7	95	5+3=8	95	2
34	211	0.29	0.85	0.69	1	TP	O	O	X	1	ER/PR^+	1	0	–	–	–	–	–
35	1772	0.52	0.81	0.08	1	ER/PR^+	O	O	O	1	ER/PR^+	1	0	5+3=8	95	5+3=8	95	2
36	743	0.42	0.96	0.47	1	TP	O	O	O	1	TP	1	1	5+3=8	95	0+0=0	0	3
37	1401	0.48	0.01	0	1	TN	O	O	O	1	TN	0	0	0+0=0	0	0+0=0	0	0
38	196	0.19	0.7	0.05	1	ER/PR^+	O	O	O	1	ER/PR^+	1	0	5+3=8	98	5+3=8	98	0
39	595	0.19	0.83	0.26	1	ER/PR^+	O	O	O	1	ER/PR^+	1	0	5+3=8	95	3+3=6	30	1
40	118	0	–	–	0		O			0		–	–	–	–	–	–	–
41	363	0.17	0.65	0.05	1	ER/PR^+	O	O	O	1	ER/PR^+	1	0	5+3=8	100	5+3=8	100	1
42	6	1	–	–	***ND***					0		–	–	–	–	–	–	–
43	5780	0.54	0.94	0.3	1	ER/PR^+	O	O	O	1	ER/PR^+	1	0	5+3=8	70	5+3=8	95	1

continued on next page

	CytoPAN (1 hour; scant cells)									Pathology (days; core immunohistochemistry)								
No.	Total count	Cancer: Quad (%)	ER/PR$^+$ (%)	HER2$^+$ (%)	Cancer dx	Sub type dx	Quad match	ER/PR match	HER2 match	Cancer dx	Sub type dx	ER/PR$^+$ status	HER$^+$ status	ER score	ER (%)	PR score	PR (%)	HER2 score
44	451	0.35	0.87	0.34	1	ER/PR$^+$	O	O	O	1	ER/PR$^+$	1	0	5+3=8	100	5+3=8	100	1
45	448	0.63	0.97	0.29	1	ER/PR$^+$	O	O	O	1	ER/PR$^+$	1	0	5+3=8	95	5+3=8	95	1
46	66	0	–	–	0		O			0		–	–	–	–	–	–	–
47	1174	0.16	0.13	0.51	1	HER2$^+$	O	O	O	1	HER2$^+$	0	1	0+0=0	0	0+0=0	0	3
48	52	0.67	0.89	0.09	1	ER/PR$^+$	O	O	O	1	ER/PR$^+$	1	0	5+3=8	98	5+3=8	90	2
49	522	0	–	–	0		O			0		–	–	–	–	–	–	–
50	3310	0.12	0.04	0.9	1	HER2$^+$	O	X	O	1	TP	1	1	2+3=5	10	2+1=3	2	3
51	21	0.1	–	–	***ND***					0		–	–	–	–	–	–	–
52	101	0.76	0.04	0.17	1	TN	O	X	O	1	ER/PR$^+$	1	0	5+3=8	95	5+2=7	95	1
53	3560	0.25	0.01	0.49	1	HER2$^+$	O	O	O	1	HER2$^+$	0	1	0+0=0	0	0+0=0	0	3
54	347	0.27	0.67	0.22	1	ER/PR$^+$	O	O	O	1	ER/PR$^+$	1	0	5+2=8	90	4+3=7	70	1
55	1590	0.14	0.61	0.02	1	ER/PR$^+$	O	O	O	1	ER/PR$^+$	1	0	5+3=8	85	3+2=5	40	1
56	520	0.02	0.75	0	***Repeat***					1	ER/PR$^+$	1	0	5+2=7	90	5+3=8	90	1
57	1576	0.26	0.79	0.25	1	ER/PR$^+$	O	O	O	1	ER/PR$^+$	1	0	5+3=8	90	5+3=8	90	2
58	2586	0	–	–	0		O			0		–	–	–	–	–	–	–
59	18	0.06	–	–	***ND***					**0**		**–**	**–**	**–**	**–**	**–**	**–**	**–**
60	722	0	–	–	0		O			0		–	–	–	–	–	–	–
61	1241	0.17	0.41	0	1	TN	O	O	O	1	TN	0	0	3+2=5	15	0+0=0	0	1
62	486	0.15	0.03	0.46	1	HER2$^+$	O	X	O	1	TP	1	1	5+3=8	95	5+3=8	90	3
63	375	0.17	0.78	0.14	1	ER/PR$^+$	O	O	O	1	ER/PR$^+$	1	0	5+3=8	90	0+0=0	0	1
64	1979	0.31	0.78	0.16	1	ER/PR$^+$	O	O	O	1	ER/PR$^+$	1	0	5+3=8	90	0+0=0	0	1
65	387	0.05	–	–	***Repeat***					**0**		**–**	**–**	**–**	**–**	**–**	**–**	**–**
66	468	0.89	0.86	0	1	ER/PR$^+$	O	O	O	1	ER/PR$^+$	1	0	5+3=8	90	0+0=0	0	1
67	735	0.7	0.71	0.03	1	ER/PR$^+$	O	O	O	1	ER/PR$^+$	1	0	3+2=5	50	3+2=5	30	0
68	334	0.67	0.8	0	1	ER/PR$^+$	O	O	O	1	ER/PR$^+$	1	0	4+1=5	70	2+2=4	10	0

cycling techniques (*42*, *43*) for deeper multiplexing. Last, there is a room for system enhancements such as including autofocusing and making the system more rugged for portable use in more extreme climates. These additional engineering aspects are straightforward to implement without adding to the overall cost of the device.

We envision that the technology could also speed up turnaround times between intervention and results in established health care systems. Given the large number of breast core biopsies in developed countries (for example, 1.6 million breast biopsies per year in the United States) with a moderate positivity rate (~20 to 25%, indicating ~1.3 million unnecessary biopsies per year) and marked morbidity and delays, it may be reasonable to explore the use of CytoPAN as an alternative strategy for faster, minimally invasive diagnostics from FNA in both developed countries and LMICs. In addition, with the use of cycling technologies (*42*, *43*), CytoPAN could be applied to additional applications such as immune cell profiling, drug trial enrollments, therapeutic efficacy testing, theranostics, or noncancer analyses such as those for hepatocytes in liver disease.

MATERIALS AND METHODS

Study design

The study was designed to develop, optimize, and validate a POC cancer diagnostic system for the analysis of breast FNA samples. We set out to develop an integrated platform with fast, automated analyses to identify malignant cells in a given FNA sample and determine the receptor status (ER/PR and HER2) of these cells. All preclinical studies were performed in replicates (typically $n = 3$, unless otherwise specified). Following staining optimization studies, reproducibility was tested on different days. Subsequently, extensive validation studies were performed using breast cancer cell lines and mouse models before the clinical study. On the basis of the mouse studies, we conducted the power analysis using two independent groups with a small effect size (TNBC and benign) to calculate the necessary clinical samples size ($n = 46$). All clinical experiments were performed in blinded fashion without knowledge of pathological information.

Cell lines

A panel of breast cancer cell lines with different expressions of triple markers (ER, PR, and HER2) was used for assay validation: MCF7, T47D, BT474, SkBr3, HCC1954, HCC1937, and MDA-MB-231. All cell lines were purchased from the American Type Culture Collection. MCF7 and MDA-MB-231 were maintained in Dulbecco's modified Eagle's medium (DMEM); SkBr3 was maintained in McCoy's 5A; and T47D, BT474, HCC1954, and HCC1937 were maintained in RPMI 1640. All media were supplemented with 10% fetal bovine serum and penicillin-streptomycin (cellgro). All cell lines were routinely tested using MycoAlert mycoplasma detection kit (Lonza).

Antibodies

Table S3 lists the antibodies used in this study. For POC operation, we further tested lyophilized antibodies. Solutions containing antibodies, 60 mM trehalose, and 0.01% polysorbate 20 in 5 mM histidine buffer at pH 6 were frozen by immersion in liquid nitrogen and then lyophilized at 4°C for 5 hours, followed by lyophilization at room temperature overnight on a VirTis Freezemobile 25EL freeze dryer (SP Scientific). The lyophilized antibodies were vacuum-sealed and then tested under different storage conditions (−20°, 4°, and 20°C). The functionality of the lyophilized antibodies was tested and compared with fresh nonlyophilized antibodies. After rehydration with distilled water, antibodies could be used without additional modifications.

System construction and automation

A low-cost white LED (Adafruit, 1622), a 365-nm LED (Thorlabs, M365D2), and lasers (405, 488, and 638 nm; CivilLaser) were used for bright-field, DAPI, Quad, HER2, and ER/PR channels, respectively. The optical imaging module consisted of an objective lens (20×, 0.70 numerical aperture; Nikon), a quad-band filter (Chroma, 89101m), and a 5-megapixel monochrome imaging sensor (The Imaging Source, DMM 37UX250-ML). The optomechanical components were either purchased from Thorlabs or built in-house using three-dimensional printing technology (Formlabs, Form 2). A microcontroller (Arduino, Arduino Nano) was used to control the light sources and a Hall effect sensor (Littelfuse, 55140-3H-02-A) for automatic image acquisition and precision positioning, respectively. The component list and cost breakdown of CytoPAN are provided in table S3. Suspended fluorescent calibration beads (Thermo Fisher Scientific, A16503 and A16504) were used to calibrate and compare image quality to a high-end upright fluorescence microscope.

User interface and image analysis

The CytoPAN user interface was based on the Visual Basic platform (Visual Studio 2019). Daily calibration, sample processing, and patient report readout were all built in a simple user interface to facilitate operation by end users. Image processing algorithms were applied for cell segmentation using bright-field and DAPI images. Briefly, the Sobel edge detection method was used to determine cellular edges based on high contrast in the bright-field image. Subsequently, the binary gradient mask underwent dilation, hole filling, and smoothing. Overlays with DAPI signals identified cell objects. Cells touching image borders were removed from analysis. Breast cancer subtypes were then classified on the basis of marker expression. For image analysis, we leveraged and integrated MATLAB dynamic-link libraries into the Visual Studio platform.

Immunostaining assay

We performed a thorough screening test for assay optimization and validation in cell lines. Specifically, we tested (i) different combinations of primary and secondary antibodies at various concentrations, (ii) different assay buffers, (iii) different staining conditions (sequence and time), and (iv) environmental influences and reagent stability. In general, harvested cells preserved in CRR (Thermo Fisher Scientific) were permeabilized with BD perm/wash buffer (BD Biosciences) for 10 min. The cells were then blocked with assay buffer supplemented with 2.5% bovine serum albumin (BSA) and 2.5% normal goat serum for 10 min. The blocking solution was removed after centrifuging at 2000*g* for 1 min. Cells were resuspended in 50 μl of assay buffer and labeled with antibodies against ER, PR, HER2, and Quad (EpCAM, EGFR, HER2, and MUC1) for 20 min, followed by a quick washing (1 ml of assay buffer added, mixture centrifuged at ~2000*g* for 1 min, and supernatant removed). Subsequently, cells were resuspended in 50 μl of assay buffer and labeled with a secondary antibody cocktail (Alexa Fluor 647 anti-rabbit IgG antibody, Alexa Fluor 488 anti-rat IgG antibody, and BV 605 anti-mouse IgG) for 10 min, followed by a quick washing. The labeled cells were then mounted on the glass surface with a mounting solution (ProLong Gold Antifade mountant with DAPI) and covered with a 12-mm round coverslip. Assay buffer was BD perm/wash buffer (BD Biosciences).

Flow cytometry

We performed flow cytometry to (i) benchmark CytoPAN measurements and (ii) validate the lyophilized antibody activity. About 10^6 cells were prepared identically to those for CytoPAN. Fluorescence signals were measured using BD LSRII Flow Cytometer (BD Biosciences) and normalized against IgG isotype controls. Data were analyzed using FlowJo software (version 10.6.0, Tree Star Inc.).

Microscopy

Fluorescence images of captured cells were acquired on an Olympus BX-63 upright automated epifluorescence microscope. All cells were stained with DAPI and visualized after capture with a DAPI filter cube. Data were analyzed using ImageJ software.

Mouse tumors

Adherent breast cancer cells were removed using 0.25% trypsin (Gibco), washed twice in 50% DMEM (without supplements) and 50% phosphate-buffered saline (PBS), and counted by a hemocytometer. Female *NOD/SCID/IL2Rg–/–* mice (10 to 12 weeks; the Jackson laboratory, no. 005557) were anesthetized by inhalation of 2% isoflurane, and their lower backs and mammary fat pads were injected subcutaneously with 2×10^6 cancer cells in 50 μl of 50% growth factor-reduced Matrigel using 0.5-ml insulin syringes. Where appropriate, 90-day slow-releasing 17b-estradiol (0.72 mg per pellet) hormone pellets (Innovative Research of America) were implanted subcutaneously in the upper back of recipient mice (*51*).

Mouse FNAs and cutoffs

Mice typically underwent FNAs 5 weeks after implantation, with individual mice receiving between two and five FNAs in total. One-milliliter syringes were prepared with 0.2 ml of CRR medium and a 22-gauge needle. Mice were anesthetized with 2% isoflurane inhalation during the FNA procedure. FNAs were harvested by inserting and withdrawing the needle within the tumor and applying slight negative pressure on the plunger of the syringe. This step was repeated two to five times per location similar to clinical procedure. FNAs were collected from three different locations in each tumor. The collected samples were flushed out of syringes with CRR medium into 1.5-ml Eppendorf tubes. The samples were washed with 2% BSA-PBS and then processed for CytoPAN analyses. All animal studies were performed in accordance with the guidelines established by the Institutional Animal Care and Use Committee at Massachusetts General Hospital (MGH).

We established reference ranges and cutoffs for each staining parameter in the mouse co-clinical study. The positive cutoffs for

biomarker expression were determined according to the conventional criterion: (mean + 2 × SD) from the marker expression profiles of IgG isotype controls. The positive cutoffs for biomarker-positive cell proportions were determined by ROC analyses. Briefly, the cells were sampled from mouse xenografts (benign and all four subtypes of malignant breast cancer from seven different human cell lines). We generated ROC curves to determine (i) the cutoffs for marker-positive cell proportions and (ii) the minimum number of cells required for accurate cancer diagnosis according to the Youden's index method.

Clinical study

The current study was designed to prospectively obtain patient samples and then correlate them with pathological and clinical information. Sample collection and processing were approved by the Institutional Review Board of the Kyungpook National University Chilgok Hospital (KNUCH 2015-05-205) with informed consent. Patients with operable breast cancer who underwent surgery at the Kyungpook National University Chilgok Hospital (Daegu, South Korea) were recruited between March 2019 and January 2020. Patients with breast cancer who had been treated with neoadjuvant chemotherapy or had prior surgery/excisional biopsies were excluded. The clinical records and pathologic results were carefully reviewed, and clinicopathological parameters were reviewed (table S4).

FNA samples were obtained as part of standard-of-care, clinically indicated image-guided biopsies of suspicious breast masses. Ultrasound-guided FNAs were performed using 21-gauge needles to yield material for CytoPAN analysis. Additional core biopsies were obtained for conventional surgical pathology and IHC workup, which served as the gold standard. FNA samples were fixed in CRR and then processed as described for cell lines. CytoPAN analyses were conducted blinded to conventional pathology and vice versa.

Quality control

All surgical operators were trained in proper FNA acquisition and sample processing. Operational quality controls occurred at several levels: (i) use of a daily quality control of laser and imaging settings with calibration beads and positive/negative cell-based test samples, (ii) stringent reagent quality control of lyophilized kits to assure antibody reactivity and consistency between lots and with each use, (iii) operator training/competency in basic laboratory skills such as pipetting and computer use (iv) a calibration routine confirming that cells on the sample slide were in the correct focal plane, and (v) a custom-designed software package (available at https://csb.mgh.harvard.edu/bme_software) to minimize bias in image interpretation.

Statistics

Statistical analyses and data plotting were performed in GraphPad Prism 7. For correlations, the linear least squares fitting was performed at the 95% confidence level, and the Pearson correlation coefficient was used to quantify the correlations between different variables. Group differences were tested using the nonparametric Mann-Whitney test for two groups and analysis of variance (ANOVA) with post hoc analysis for more than two groups. ROC curves were constructed for individual markers to describe the accuracy for cancer detection and subtyping. The cutoff points were selected using Youden's index, which maximizes the sum of sensitivity and specificity. The power analysis for Mann-Whitney test was performed using G*Power to compute the necessary clinical sample size given the statistical power $(1 - \beta)$ of 0.9, the effect size of 1.77, and the allocation ratio n_{cancer}/n_{benign} of 0.1. All tests were two sided, and $P < 0.05$ was considered statistically significant.

SUPPLEMENTARY MATERIALS

stm.sciencemag.org/cgi/content/full/12/555/eaaz9746/DC1
Fig. S1. Comparison of conventional pathology and CytoPAN.
Fig. S2. CytoPAN readouts for comixtures of benign and malignant cells.
Fig. S3. Decision tree algorithm to classify cell populations.
Fig. S4. Selection of optimal fixation methods for FNA specimen.
Fig. S5. Selection of optimal permeabilization methods.
Fig. S6. Comparison of direct staining (one-step) and indirect staining (two-step).
Fig. S7. Stability test for lyophilized antibodies.
Fig. S8. Bleed-through analyses and signal deconvolution.
Fig. S9. CytoPAN user interface.
Fig. S10. System characterization.
Fig. S11. Comparison of CytoPAN and flow cytometry for different cell lines.
Fig. S12. Comparison of CytoPAN and flow cytometry for repeat FNA from mice bearing four different breast tumor types.
Fig. S13. Statistical analyses to determine cutoffs.
Fig. S14. Quad as a cancer marker.
Table S1. Pairs of primary and fluorophore-conjugated, species-specific secondary antibodies used in the study.
Table S2. Cost of CytoPAN device.
Table S3. Antibody list and cost for human samples.
Table S4. Summary of patient cohort.
Data file S1.

View/request a protocol for this paper from *Bio-protocol*.

REFERENCES AND NOTES

1. F. Bray, J. Ferlay, I. Soerjomataram, R. L. Siegel, L. A. Torre, A. Jemal, Global cancer statistics 2018: Globocan estimates of incidence and mortality worldwide for 36 cancers in 185 countries. *CA Cancer J. Clin.* **68**, 394–424 (2018).
2. S. McGuire, World cancer report 2014. Geneva, Switzerland: World health organization, international agency for research on cancer, WHO press, 2015. *Adv. Nutr.* **7**, 418–419 (2016).
3. L. N. Shulman, W. Willett, A. Sievers, F. M. Knaul, Breast cancer in developing countries: Opportunities for improved survival. *J. Oncol.* **2010**, 595167 (2010).
4. M. H. Forouzanfar, K. J. Foreman, A. M. Delossantos, R. Lozano, A. D. Lopez, C. J. Murray, M. Naghavi, Breast and cervical cancer in 187 countries between 1980 and 2010: A systematic analysis. *Lancet* **378**, 1461–1484 (2011).
5. M. Fish, J. Parkes, N. Dharsee, S. Dryden-Peterson, J. Efstathiou, L. Schnipper, B. Chabner, A. R. Parikh, Poetic (program for enhanced training in cancer): An initial experience of supporting capacity building for oncology training in sub-Saharan Africa. *Oncologist* **24**, 1557–1561 (2019).
6. H. S. Iyer, R. E. Kohler, D. Ramogola-Masire, C. Brown, K. Molebatsi, S. Grover, I. Kablay, M. Bvochora-Nsingo, J. A. Efstathiou, S. Lockman, N. Tapela, S. L. Dryden-Peterson, Explaining disparities in oncology health systems delays and stage at diagnosis between men and women in Botswana: A cohort study. *PLOS ONE* **14**, e0218094 (2019).
7. J. Makhema, K. E. Wirth, M. P. Holme, T. Gaolathe, M. Mmalane, E. Kadima, U. Chakalisa, K. Bennett, J. Leidner, K. Manyake, A. M. Mbikiwa, S. V. Simon, R. Letlhogile, K. Mukokomani, E. van Widenfelt, S. Moyo, R. Lebelonyane, M. G. Alwano, K. M. Powis, S. L. Dryden-Peterson, C. Kgathi, V. Novitsky, J. Moore, P. Bachanas, W. Abrams, L. Block, S. El-Halabi, T. Marukutira, L. A. Mills, C. Sexton, E. Raizes, S. Gaseitsiwe, H. Bussmann, L. Okui, O. John, R. L. Shapiro, S. Pals, H. Michael, M. Roland, V. DeGruttola, Q. Lei, R. Wang, E. T. Tchetgen, M. Essex, S. Lockman, Universal testing, expanded treatment, and incidence of HIV infection in Botswana. *N. Engl. J. Med.* **381**, 230–242 (2019).
8. A. M. Nelson, D. A. Milner, T. R. Rebbeck, Y. Iliyasu, Oncologic care and pathology resources in Africa: Survey and recommendations. *J. Clin. Oncol.* **34**, 20–26 (2016).
9. World Health Organization, www.who.int/en/news-room/fact-sheets/detail/cancer (2018).
10. Early Breast Cancer Trialists' Collaborative Group (EBCTCG), C. Davies, J. Godwin, R. Gray, M. Clarke, D. Cutter, S. Darby, P. McGale, H. C. Pan, C. Taylor, Y. C. Wang, M. Dowsett, J. Ingle, R. Peto, Relevance of breast cancer hormone receptors and other factors to the efficacy of adjuvant tamoxifen: Patient-level meta-analysis of randomised trials. *Lancet* **378**, 771–784 (2011).

11. Y. T. Bazargani, A. de Boer, J. H. Schellens, H. G. Leufkens, A. K. Mantel-Teeuwisse, Essential medicines for breast cancer in low and middle income countries. *BMC Cancer* **15**, 591 (2015).
12. V. Vanderpuye, S. Grover, N. Hammad, PoojaPrabhakar, H. Simonds, F. Olopade, D. C. Stefan, An update on the management of breast cancer in Africa. *Infect. Agent Cancer* **12**, 13 (2017).
13. J. B. Haun, C. M. Castro, R. Wang, V. M. Peterson, B. S. Marinelli, H. Lee, R. Weissleder, Micro-NMR for rapid molecular analysis of human tumor samples. *Sci. Transl. Med.* **3**, 71ra16 (2011).
14. S. Jeong, J. Park, D. Pathania, C. M. Castro, R. Weissleder, H. Lee, Integrated magneto-electrochemical sensor for exosome analysis. *ACS Nano* **10**, 1802–1809 (2016).
15. H. Im, H. Shao, Y. I. Park, V. M. Peterson, C. M. Castro, R. Weissleder, H. Lee, Label-free detection and molecular profiling of exosomes with a nano-plasmonic sensor. *Nat. Biotechnol.* **32**, 490–495 (2014).
16. K. S. Yang, H. Im, S. Hong, I. Pergolini, A. F. Del Castillo, R. Wang, S. Clardy, C. H. Huang, C. Pille, S. Ferrone, R. Yang, C. M. Castro, H. Lee, C. F. Del Castillo, R. Weissleder, Multiparametric plasma EV profiling facilitates diagnosis of pancreatic malignancy. *Sci. Transl. Med.* **9**, eaal3226 (2017).
17. H. Im, D. Pathania, P. J. McFarland, A. R. Sohani, I. Degani, M. Allen, B. Coble, A. Kilcoyne, S. Hong, L. Rohrer, J. S. Abramson, S. Dryden-Peterson, L. Fexon, M. Pivovarov, B. Chabner, H. Lee, C. M. Castro, R. Weissleder, Design and clinical validation of a point-of-care device for the diagnosis of lymphoma via contrast-enhanced microholography and machine learning. *Nat. Biomed. Eng.* **2**, 666–674 (2018).
18. J. Min, H. Im, M. Allen, P. J. McFarland, I. Degani, H. Yu, E. Normandin, D. Pathania, J. M. Patel, C. M. Castro, R. Weissleder, H. Lee, Computational optics enables breast cancer profiling in point-of-care settings. *ACS Nano* **12**, 9081–9090 (2018).
19. R. S. Gaster, D. A. Hall, C. H. Nielsen, S. J. Osterfeld, H. Yu, K. E. Mach, R. J. Wilson, B. Murmann, J. C. Liao, S. S. Gambhir, S. X. Wang, Matrix-insensitive protein assays push the limits of biosensors in medicine. *Nat. Med.* **15**, 1327–1332 (2009).
20. H. Shafiee, W. Asghar, F. Inci, M. Yuksekkaya, M. Jahangir, M. H. Zhang, N. G. Durmus, U. A. Gurkan, D. R. Kuritzkes, U. Demirci, Paper and flexible substrates as materials for biosensing platforms to detect multiple biotargets. *Sci. Rep.* **5**, 8719 (2015).
21. C. K. Tang, A. Vaze, M. Shen, J. F. Rusling, High-throughput electrochemical microfluidic immunoarray for multiplexed detection of cancer biomarker proteins. *ACS Sens.* **1**, 1036–1043 (2016).
22. L. Wang, Q. Xiong, F. Xiao, H. Duan, 2D nanomaterials based electrochemical biosensors for cancer diagnosis. *Biosens. Bioelectron.* **89**, 136–151 (2017).
23. S. Chakravarty, W. C. Lai, Y. Zou, H. A. Drabkin, R. M. Gemmill, G. R. Simon, S. H. Chin, R. T. Chen, Multiplexed specific label-free detection of NCI-H358 lung cancer cell line lysates with silicon based photonic crystal microcavity biosensors. *Biosens. Bioelectron.* **43**, 50–55 (2013).
24. F. Liang, N. Clarke, P. Patel, M. Loncar, Q. Quan, Scalable photonic crystal chips for high sensitivity protein detection. *Opt. Express* **21**, 32306–32312 (2013).
25. C. S. Huang, V. Chaudhery, A. Pokhriyal, S. George, J. Polans, M. Lu, R. Tan, R. C. Zangar, B. T. Cunningham, Multiplexed cancer biomarker detection using quartz-based photonic crystal surfaces. *Anal. Chem.* **84**, 1126–1133 (2012).
26. A. Greenbaum, N. Akbari, A. Feizi, W. Luo, A. Ozcan, Field-portable pixel super-resolution colour microscope. *PLOS ONE* **8**, e76475 (2013).
27. D. Mabey, R. W. Peeling, A. Ustianowski, M. D. Perkins, Diagnostics for the developing world. *Nat. Rev. Microbiol.* **2**, 231–240 (2004).
28. G. Wu, M. H. Zaman, Low-cost tools for diagnosing and monitoring hiv infection in low-resource settings. *Bull. World Health Organ.* **90**, 914–920 (2012).
29. N. E. Frenk, L. Spring, A. Muzikansky, H. V. Vadvala, J. M. Gurski Jr., L. E. Henderson, M. Mino-Kenudson, A. Ly, A. Bardia, D. Finkelstein, J. Engelman, P. M. Mueller, D. Juric, R. Weissleder, High-content biopsies facilitate molecular analyses and do not increase complication rates in patients with advanced solid tumors. *JCO Precis. Oncol.* **1**, 1–9 (2017).
30. C. A. Brown, G. Suneja, N. Tapela, A. Mapes, M. Pusoentsi, M. Mmalane, R. Hodgeman, M. Boyer, Z. Musimar, D. Ramogola-Masire, S. Grover, M. Nsingo-Bvochora, M. Kayembe, J. Efstathiou, S. Lockman, S. Dryden-Peterson, Predictors of timely access of oncology services and advanced-stage cancer in an HIV-endemic setting. *Oncologist* **21**, 731–738 (2016).
31. C. M. Castro, A. A. Ghazani, J. Chung, H. Shao, D. Issadore, T. J. Yoon, R. Weissleder, H. Lee, Miniaturized nuclear magnetic resonance platform for detection and profiling of circulating tumor cells. *Lab Chip* **14**, 14–23 (2014).
32. A. A. Ghazani, S. McDermott, M. Pectasides, M. Sebas, M. Mino-Kenudson, H. Lee, R. Weissleder, C. M. Castro, Comparison of select cancer biomarkers in human circulating and bulk tumor cells using magnetic nanoparticles and a miniaturized micro-NMR system. *Nanomedicine* **9**, 1009–1017 (2013).
33. P. Wirapati, C. Sotiriou, S. Kunkel, P. Farmer, S. Pradervand, B. Haibe-Kains, C. Desmedt, M. Ignatiadis, T. Sengstag, F. Schütz, D. R. Goldstein, M. Piccart, M. Delorenzi, Meta-analysis of gene expression profiles in breast cancer: Toward a unified understanding of breast cancer subtyping and prognosis signatures. *Breast Cancer Res.* **10**, R65 (2008).
34. L. L. Lanier, N. L. Warner, Paraformaldehyde fixation of hematopoietic cells for quantitative flow cytometry (FACS) analysis. *J. Immunol. Methods* **47**, 25–30 (1981).
35. G. Schmitz, G. Rothe, A. Ruf, S. Barlage, D. Tschöpe, K. J. Clemetson, A. H. Goodall, A. D. Michelson, A. T. Nurden, T. V. Shankey, European working group on clinical cell analysis: Consensus protocol for the flow cytometric characterisation of platelet function. *Thromb. Haemost.* **79**, 885–896 (1998).
36. W. Wang, S. Singh, D. L. Zeng, K. King, S. Nema, Antibody structure, instability, and formulation. *J. Pharm. Sci.* **96**, 1–26 (2007).
37. H. Inan, M. Poyraz, F. Inci, M. A. Lifson, M. Baday, B. T. Cunningham, U. Demirci, Photonic crystals: Emerging biosensors and their promise for point-of-care applications. *Chem. Soc. Rev.* **46**, 366–388 (2017).
38. M. Zarei, Advances in point-of-care technologies for molecular diagnostics. *Biosens. Bioelectron.* **98**, 494–506 (2017).
39. P. Wang, L. J. Kricka, Current and emerging trends in point-of-care technology and strategies for clinical validation and implementation. *Clin. Chem.* **64**, 1439–1452 (2018).
40. T. P. Kingham, O. I. Alatise, V. Vanderpuye, C. Casper, F. A. Abantanga, T. B. Kamara, O. I. Olopade, M. Habeebu, F. B. Abdulkareem, L. Denny, Treatment of cancer in sub-Saharan Africa. *Lancet Oncol.* **14**, e158–e167 (2013).
41. T. S. Kline, H. S. Neal, Needle aspiration biopsy: A critical appraisal. Eight years and 3,267 specimens later. *JAMA* **239**, 36–39 (1978).
42. J. Ko, J. Oh, M. S. Ahmed, J. C. T. Carlson, R. Weissleder, Ultra-fast cycling for multiplexed cellular fluorescence imaging. *Angew. Chem. Int. Ed. Eng.* **59**, 6839–6846 (2020).
43. R. J. Giedt, D. Pathania, J. C. T. Carlson, P. J. McFarland, A. F. Del Castillo, D. Juric, R. Weissleder, Single-cell barcode analysis provides a rapid readout of cellular signaling pathways in clinical specimens. *Nat. Commun.* **9**, 4550 (2018).
44. A. N. Marquard, J. C. T. Carlson, R. Weissleder, Glass chemistry to analyze human cells under adverse conditions. *ACS Omega* **4**, 11515–11521 (2019).
45. P. L. Cheah, L. M. Looi, S. Horton, Cost analysis of operating an anatomic pathology laboratory in a middle-income country. *Am. J. Clin. Pathol.* **149**, 1–7 (2017).
46. J. F. Nasuti, P. K. Gupta, Z. W. Baloch, Diagnostic value and cost-effectiveness of on-site evaluation of fine-needle aspiration specimens: Review of 5,688 cases. *Diagn. Cytopathol.* **27**, 1–4 (2002).
47. M. Rajer, M. Kmet, Quantitative analysis of fine needle aspiration biopsy samples. *Radiol. Oncol.* **39**, 269–272 (2005).
48. H. Cubasch, M. Joffe, R. Hanisch, J. Schuz, A. I. Neugut, A. Karstaedt, N. Broeze, E. van den Berg, V. McCormack, J. S. Jacobson, Breast cancer characteristics and HIV among 1,092 women in Soweto, South Africa. *Breast Cancer Res. Treat.* **140**, 177–186 (2013).
49. S. Chirkut, Breast cancer, human immunodeficiency virus and highly active antiretroviral treatment; implications for a high-rate seropositive region. *Oncol. Rev.* **13**, 376 (2019).
50. R. K. Bhatia, M. Narasimhamurthy, Y. M. Martei, P. Prabhakar, J. Hutson, S. Chiyapo, I. Makozhombwe, M. Feldman, M. K. A. Kayembe, K. Cooper, S. Grover, Report of clinico-pathological features of breast cancer in HIV-infected and uninfected women in Botswana. *Infect. Agents Cancer* **14**, 28 (2019).
51. H. Mohammed, I. A. Russell, R. Stark, O. M. Rueda, T. E. Hickey, G. A. Tarulli, A. A. Serandour, A. A. Serandour, S. N. Birrell, A. Bruna, A. Saadi, S. Menon, J. Hadfield, M. Pugh, G. V. Raj, G. D. Brown, C. D'Santos, J. L. Robinson, G. Silva, R. Launchbury, C. M. Perou, J. Stingl, C. Caldas, W. D. Tilley, J. S. Carroll, Progesterone receptor modulates erα action in breast cancer. *Nature* **523**, 313–317 (2015).

Acknowledgments: We would like to acknowledge extensive discussions with J. Carlson and J. Higgins. We also thank the entire Harvard/Botswana UH3 team, especially B. Chabner, S. D. Petersen, and M. Dykstra, for valuable discussions and support. **Funding:** We acknowledge the following grant support: NIH UH3 CA202637 to R.W., U01CA206997 to R.W., R01CA204019 to R.W., R01CA206890 to R.W., R33CA202064 to R.W., R01CA229777 to H.L., U01CA233360 to H.L. and C.M.C., DOD-W81XWH1910199 to H.L., MGH Scholar fund to H.L., R00CA201248 to H.I., R21CA217662 to H.I., Robert Wood Johnson Foundation to C.M.C., and NRFCRP13-2014-01 to A.-Q.L. **Author contributions:** R.W., H.I., H.L., and C.M.C. designed the study. J.M. L.K.C., and J.O. conducted the experiments. L.K.C., C.L., H.L., H.I., C.V., and A.-Q.L. developed the instrument. L.K.C., C.L., and H.I. developed the software and algorithms. J.L., S.J.L., and J.Y.P. collected the clinical samples and obtained the pathology

reports. All authors analyzed the results. J.M., L.K.C., H.L., H.I., and R.W. wrote the manuscript. All authors edited the manuscript. **Competing interests:** R.W. is a consultant to ModeRNA, Tarveda, Accure Health, Aikili, and Lumicell. H.L. is a consultant to Accure Health and Aikili. H.I. is a consultant to Noul and Aikili. C.M.C. is a consultant to Aikili. J.M. is a consultant to Aikili. The other authors declare that they have no competing interests. **Data and materials availability:** All data needed to evaluate the conclusions in the paper are present in the paper and/or the Supplementary Materials. Materials are available upon request by contacting the corresponding authors. The codes for image analysis are available at https://csb.mgh.harvard.edu/bme_software.

Submitted 24 October 2019
Resubmitted 06 March 2020
Accepted 19 June 2020
Published 5 August 2020
10.1126/scitranslmed.aaz9746

Citation: J. Min, L. K. Chin, J. Oh, C. Landeros, C. Vinegoni, J. Lee, S. J. Lee, J. Y. Park, A.-Q. Liu, C. M. Castro, H. Lee, H. Im, R. Weissleder, CytoPAN—Portable cellular analyses for rapid point-of-care cancer diagnosis. *Sci. Transl. Med.* **12**, eaaz9746 (2020).

Science Translational Medicine

CytoPAN—Portable cellular analyses for rapid point-of-care cancer diagnosis

Jouha Min, Lip Ket Chin, Juhyun Oh, Christian Landeros, Claudio Vinegoni, Jeeyeon Lee, Soo Jung Lee, Jee Young Park, Ai-Qun Liu, Cesar M. Castro, Hakho Lee, Hyungsoon Im and Ralph Weissleder

Sci Transl Med **12**, eaaz9746.
DOI: 10.1126/scitranslmed.aaz9746

Panning for diagnostic gold

Accurate and timely diagnosis and categorization of cancer are not always simple even under optimal conditions, and it can be near impossible in the developing world, where the necessary specialists and equipment may not be available and biopsy results can take months to return. To address this diagnostic bottleneck, Min *et al.* devised an automated image cytometry system named CytoPAN, which can correctly detect breast cancer and identify its subtype in 1 hour using samples obtained by fine needle aspiration, a less invasive technique than core biopsy. The system is relatively affordable and requires minimal training, which should decrease the barriers to access in low-resource areas.